J Opt (September 2022) 51(3):591–604
https://doi.org/10.1007/s12596-021-00811-x

RESEARCH ARTICLE

Performance evaluation of phase plate and deformable mirror for adaptive optics (AO) system

Venkata Suresh Narra[1] · Sreekanth Reddy Vallapureddy[1] · Ravinder Kumar Banyal[1] · Raghavendra Prasad Budihal[1]

Received: 11 June 2021 / Accepted: 4 December 2021 / Published online: 30 January 2022

Abstract Spatial resolution of the ground-based optical telescopes is limited by the Earth's atmospheric turbulence rather than the size of the telescope aperture. To restore the performance of a telescope to near diffraction limit, adaptive optics (AO) system should be designed and developed based on the turbulence characteristics at the telescope site. Crucial part in developing the AO system is, simulating the turbulence conditions of the atmosphere, estimation of its effect on wavefront and correction of the distorted wavefront in the laboratory. The essential components of laboratory AO system are phase plate and deformable mirrors (DMs). Phase plate simulates the turbulent conditions, and DM corrects the distorted wavefront. Performance of AO system depends on the characterization of these two devices. Fizeau interferometer and Shack–Hartmann wavefront sensor (SHWS) are used for the performance evaluation. Current work provides a detailed discussion about the tests carried out to characterize these two components and the results obtained.

Keywords Atmospheric turbulence · Adaptive optics · Wavefront distortions · Deformable mirror (DM) · Phase plate

✉ Venkata Suresh Narra
venkata@iiap.res.in

Raghavendra Prasad Budihal
brp@iiap.res.in

[1] Indian Institute of Astrophysics, 2nd Block Koramangala, Bangalore, India

Introduction

Spatial and temporal variation of temperature across different layers of the Earth's atmosphere results in fluctuations in the refractive index. Fluctuations in the refractive index of the medium cause distortions to the wavefront of light that passes through it. Due to this, ground-based astronomical observations result in poor resolution irrespective of size of aperture of the telescope [1, 2]. Thus, Earth's atmosphere limits the performance of the telescope and restricts to atmospheric seeing limited resolution [3, 4].

Adaptive optics (AO) system corrects the wavefronts in real time and improves the performance of the telescopes [5]. To develop such system, well-controlled laboratory conditions that mimic the atmospheric turbulence are essential. In this regard, phase plate and deformable mirror (DM) are two important subcomponents of the AO system. Calibration of these components is necessary for their optimal utilization [6]. A Fizeau interferometer and Shack–Hartmann wavefront sensor (SHWS) are used for calibration. Current paper discusses the details of calibration tests carried out on phase plate and DM and discusses the results.

Calibration using Fizeau interferometer

Zygo Dynafiz [7], a high-resolution interferometer, is used to calibrate phase plate and DM [8]. It is an instantaneous Fizeau-type interferometer [9] optimized for dynamic metrology in the presence of extreme vibrations and air turbulence in the laboratory. The Mx software and live phase enable real-time analysis and dynamic testing of surfaces. DynaPhase measurement wizard with integrated calibration using Quick Fringe Acquisition System (QFAS)

and twin spot reticule enables the long cavity measurements under turbulent atmosphere. The instrument is equipped with a stabilized He-Ne laser of 633 nm wavelength, a high-resolution camera of 1200x1200 pixels with pixel size of 5.5 μm with 10 bit digital resolution. The RMS wavefront repeatability of the instrument is ~ 1 nm as shown in Fig. 1.

Phase plate calibration

Phase plates introduce random distortions to the wavefront of light passing through it. These are widely used as turbulence generators in laboratory for AO system development. Phase plate from Lexitek Inc with model number LS100 is used to simulate the random atmospheric turbulent conditions in the laboratory [10]. It is a pseudo-random phase plate created by using Near Index Match (NIM) technique. The principle behind NIM optics is illustrated in Fig. 2. Two different materials with refractive indices n_1 and n_2 that are similar but unequal are sandwiched together to form a surface profile $h(x)$ at the interface of the two materials. If the exterior surfaces of both materials are planar, then the optical path difference (OPD) impressed upon a plane wavefront is given by the following equations [10].

$$\mathrm{OPD}(x) = h(x)(n_1(\lambda) - n_2(\lambda)), \quad (1)$$

$$\mathrm{OPD}(x) = h(x)(D_n(\lambda)), \quad (2)$$

The sandwiched surface is machined with a designed OPD scaled by $1/n$, where n is the OPD scale size in terms of μm. This interface induces random OPD to the wavefront. A rotating phase plate can simulate a distributed turbulence layer. For materials with refractive index difference $\Delta n \sim 0.02$, a relief height of 50λ is required to produce an OPD of 1λ. The spatial length over which the phase plate induces distortions in the wavefront influences the sampling size for sensing. For development of AO system, it is essential to know the spatial length of the distortions introduced by the phase plate.

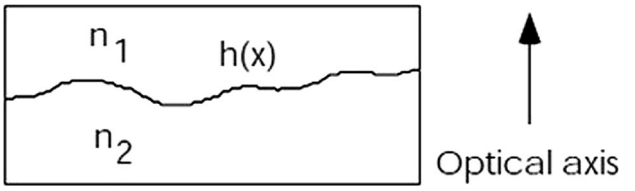

Fig. 2 Phase plate consisting of sandwich of two different materials of refractive indices of n_1 and n_2

The size of phase plate is 100 mm in diameter. It has an aberration corrected surface ~ 3 cm in diameter at the center with surface quality of $\lambda/30$ as shown in Fig. 3. Peak-to-valley (PV) and root-mean-square (RMS) value of the OPD is concerned parameters for calibration. The PV and RMS determine global tilt and mean approximation of the local tilt of the wavefront, respectively. In this exercise, the phase plate characteristics are measured for its full surface and for a subregion at different locations. For most of the AO systems, the size of the wavefront is brought down to a few millimeters, because of various constraints by other system elements such as size of SHWS, DM and the compactness of AO system. Thus, to determine the characteristics of the phase plate, a zone of 20 mm diameter is considered, which meets the requirements of the AO system.

Figure 3 shows the phase plate characteristics. The full phase plate has a PV wavefront error of 13.8 μm and RMS wavefront error of 2 μm. For the full phase plate, the beam size is in the order of 100 mm. The subregion of 20 mm shown in Fig. 3 has PV of 1.368 μm and RMS of 0.256 μm.

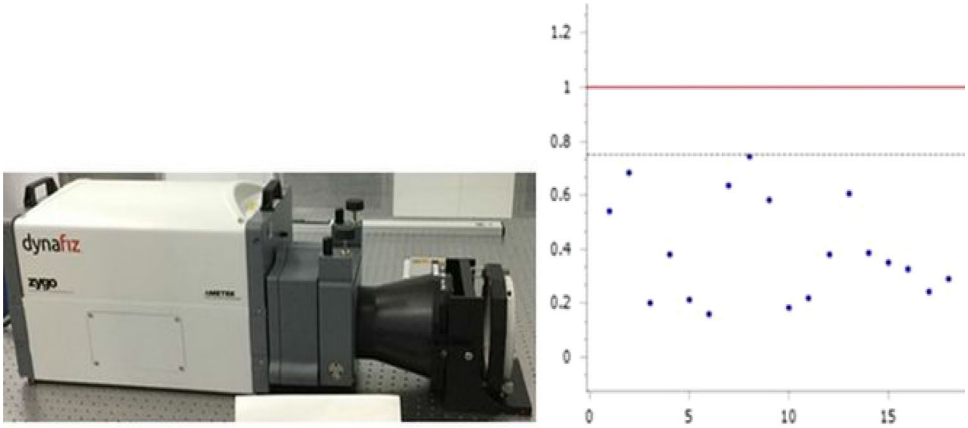

Fig. 1 Zygo Dynafiz interferometer (left). The graph in the right shows the wavefront error measured by Zygo on a test surface. The horizontal axis (H-axis) is the number of sample tests, and the vertical axis (V-axis) is the wavefront error in nm

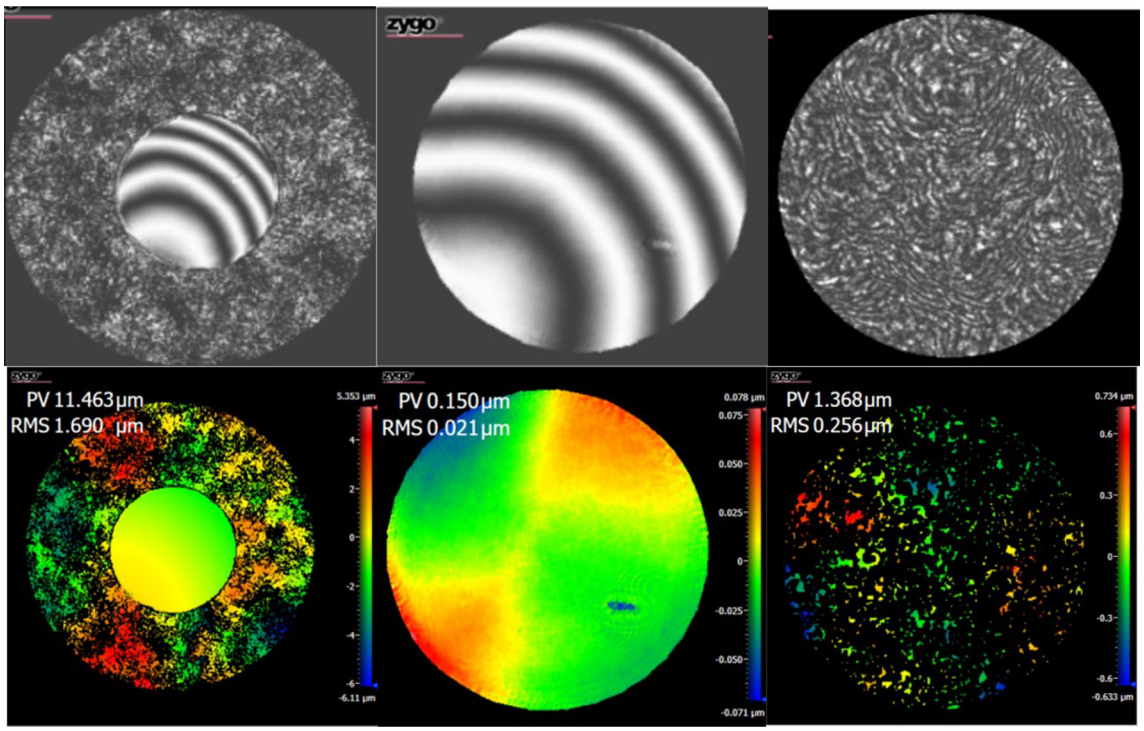

Fig. 3 Phase plate calibration result: Interferograms (top) and wavefront maps (bottom) of full plate (**a**), central part (**b**) and subregion (**c**)

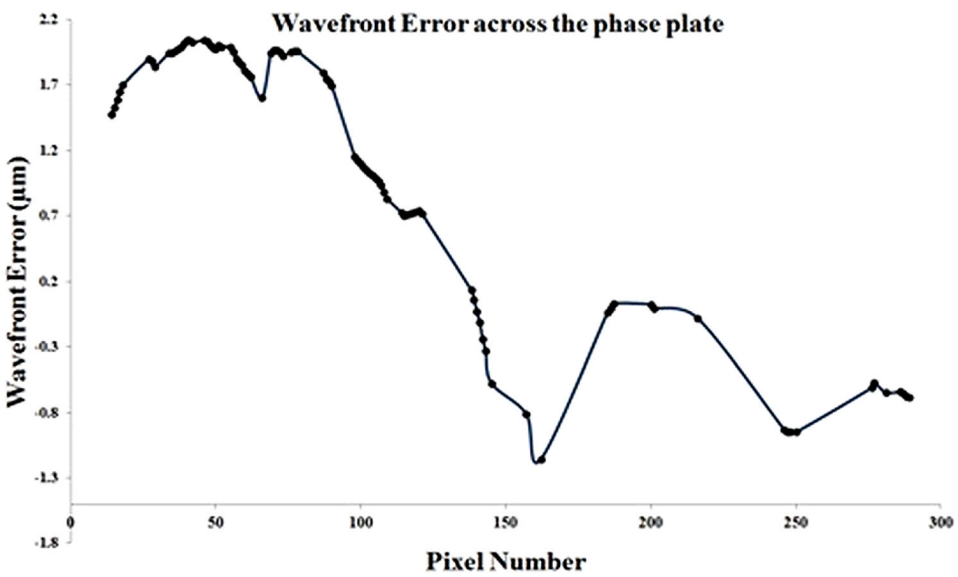

Fig. 4 Variation in wavefront error across the phase plate

Figure 4 shows the variations in wavefront error across the full plate. The plot is significant to visualize the dynamics of the wavefront phase. Ideally, it is desirable to have a continuous plot. But the scattered dots in the plot are due to a path difference of more than $\lambda/2$ between two subsequent pixels. The path difference across the zone of size 20 mm is approximately 0.236-1.56 µm. It is one of the crucial parameters to be known to set up an AO system in laboratory.

The relation between RMS wavefront error and Fried's parameter (r_o) can be expressed as [2, 11],

$$\sigma^2 = 0.132\left(\frac{D}{r_0}\right)^{5/3}, \tag{3}$$

where σ is the RMS wavefront error, D is the diameter of the telescope, and r_o is the Fried's parameter.

$$r_o = D\left(\frac{\sigma^2}{0.132}\right)^{-3/5}, \tag{4}$$

$$r_o = 1.3\left(\left(\frac{2\pi}{\lambda} * 0.236 * 10^{-6}\right) * \frac{1}{0.132}\right)^{-3/5}, \tag{5}$$

where λ is wavelength of light. Assuming the re-imaged pupil size of 4.5 mm on DM corresponds to $\sim$1 meter primary aperture of telescope, it can be said that the phase plate can introduce phase errors corresponding of 12.19 cm on telescope.

The estimated RMS error that can be induced by phase plate is 0.236-1.56 μm. The seeing parameter (r_o) that can be simulated by phase plate is 1.44-13.8 cm. This value is obtained for a telescope aperture size of 1.3 m and for a wavelength of 0.63 μm. This corresponds to a pupil size on phase plate $\sim$ 5 mm. A larger range of phase error can be obtained by selecting a larger area over phase plate.

Deformable mirror (DM) calibration

Deformable mirrors (DMs) are flexible mirrors etched with actuators to control its surface. There are different types of DMs based on mirror type such as segmented or continuous and based on the actuation technology either piezoactuators or MEMS (microelectromechanical systems)-based actuators [12, 13]. In this paper, calibration of Boston Multi-5.5 DM is discussed. It has a resolution of 0.5 nm and dynamic range of 5 μm. The DM has a thin membrane mirror of area 5x5 mm, etched with 140 electrostatic actuators with pitch size of 450 μm.

DM changes its shape in response to the position commands in order to compensate for the aberrations measured by wavefront sensor. Ideally, it will assume a surface shape that can compensate for aberration profile. The surface profile is controlled by actuators that move in and out, in response to the applied voltage. The accuracy of the wavefront correction is dependent on shaping of the DM. The range of wavefront that can be corrected by a particular DM is limited by the actuator stroke and resolution, the number and distribution of actuators and the model used to determine the appropriate control signals for the DM. First two are physical limitations of the DM itself, and last one is a limitation of the control software. The inadequate actuator stroke leads to poor performance and can prevent the effective correction. The number of actuators determines the degrees of freedom that the DM can correct.

The DM used for calibration has continuous membrane mirror. The actuators are mechanically coupled. Therefore, when an actuator moves, there is some finite response along the entire surface of the mirror. The 2D shape of the surface caused by displacing one actuator is called the influence function of that actuator. Typically, the coupling for continuous membrane DM will be in the range of 10-20%. It is desired to determine the actuators response to input voltage, inter-actuator coupling, relaxed shape error of the DM, RMS and PV wavefront error of DM surface at different voltages.

Experimental procedure

Experimental setup used to characterize the DM is shown in Fig. 5. DM is placed in front of the Fizeau interferometer from Zygo Corporation, and a neutral density (ND) filter is placed in between them. ND filter serves twin purposes here: One is protecting the DM from high intensity laser beam which may cause irretrievable damage to the DM, and other is to reduce the intensity of the reflected wavefront from DM for accurate measurements. Measured surface profiles of DM are shown in Figs. 6 and 7.

DM surface flatness is crucial for the wavefront correction. It is desirable to have a flat surface with RMS surface figure $\lambda/20$. In a relaxed stage or at an offset voltage, the DM needs to be tested for its surface flatness. It is tested for different input voltages ranging from 0 to 200 V. (Voltage applied to all the actuators is uniform.) Variation in RMS wavefront error of DM for input voltages from 0 to 200 V is in the order of 22 to 34 nm. The results are shown in Fig. 8.

Estimation of response of each actuator for input voltage is essential. All the actuators are tested over a voltage range of 90 V with an interval of 6 V. The response of the each actuator is studied.

The voltage vs PV and RMS wavefront error of the surface shows the linear displacement in the mirror along the transverse direction. The response shows the accuracy of the actuator movement with input voltage.

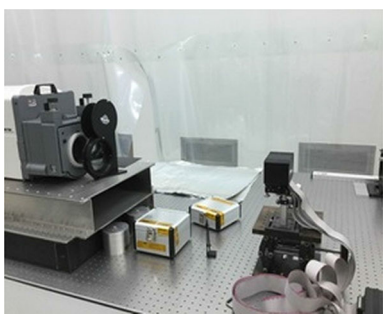

Fig. 5 Experimental setup used for calibration of DM

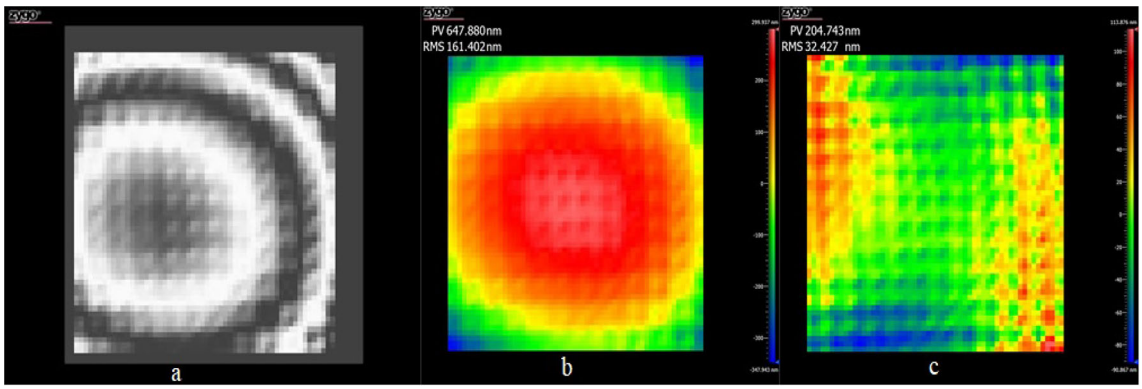

Fig. 6 Interferogram (**a**), wavefront map with power (**b**) and wavefront map without power (**c**) of DM surface in relaxed condition of the actuators

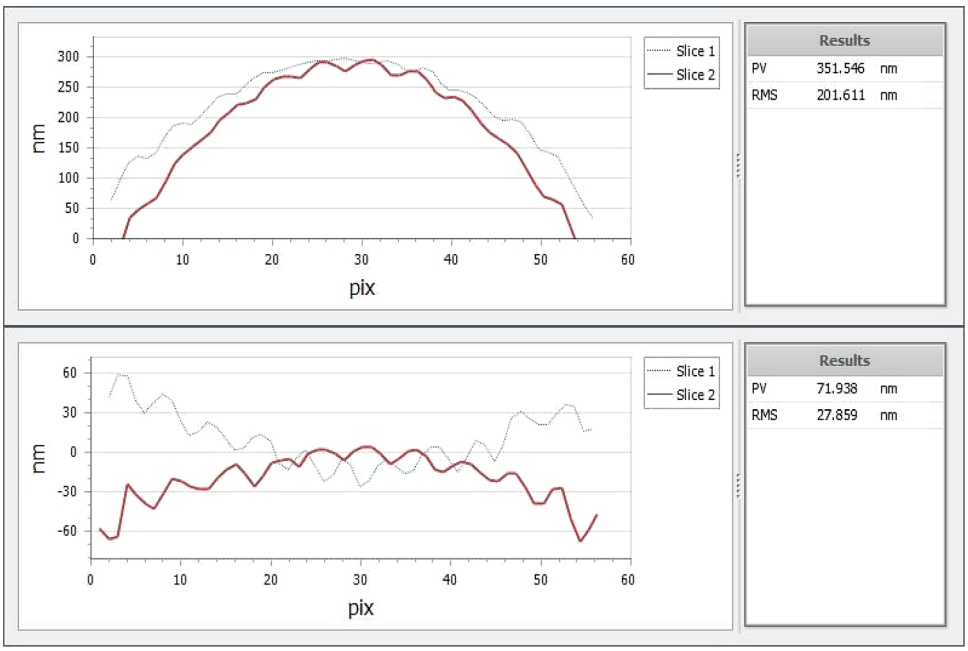

Fig. 7 One-dimensional plots of the wavefront map along H (slice 1) and V (slice 2) axis of the DM surface with (top) and without (bottom) power

In Table 1, the position map of the actuators on DM is shown and their respective position is mentioned. The response of the actuators in the prescribed voltage range of 60-90 V is given in Fig. 9. For voltages greater than 90 V, the path difference between two subsequent pixels is more than $\lambda/2$. This results in loss of phase information. Thus, we limited the analysis to 90 V. For equal response of all the actuators, the plots should have been overlapped. But there is constant offset present in the actuator response.

The response of individual actuator is different for the same input voltage. Each actuator has its unique response function. Thus, it is crucial to extract the response function of the individual actuators. To estimate this, each actuator is tested individually over a voltage range of 0-90 V. To do this, for a given input voltage, the PV and RMS surface error of the DM is measured. In a relaxed position (at 0 V input), PV and RMS surface error of the DM is $\sim$250 nm and $\sim$30 nm, respectively. Beyond an applied voltage of 90 V, the actuator response is $>$ 600 nm which is saturation stage. For better estimation of the response function, the actuators have been examined between 60-90 V. In Fig. 9, the PV and RMS of the wavefront are plotted against the input voltage. In Fig. 9, a selective set of actuators response is shown. The actuators and their corresponding position can be seen in the layout map of DM shown in Table 1. The same test was repeated for each actuator.

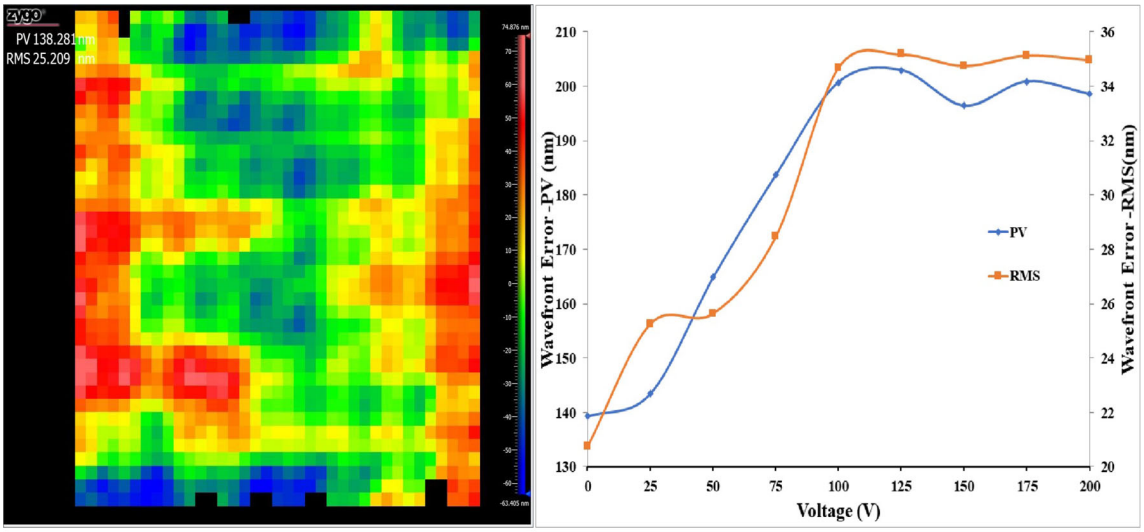

Fig. 8 DM surface map for input piston voltage of 100 V (**a**), PV and RMS wavefront error for different voltages (**b**)

Table 1 Layout of the deformable mirror actuators. DM has 140 actuators in a grid of 12x12 that covers 4.95x4.95 mm on DM surface in length and width. The four corner actuators are dormant which are not numbered. The window covers actuators of 9x9 that is 4x4 mm

	1	2	3	4	5	6	7	8	9	10	
11	12	13	14	15	16	17	18	19	20	21	22
23	24	25	26	27	28	29	30	31	32	33	34
35	36	37	38	39	40	41	42	43	44	45	46
47	48	49	50	51	52	53	54	55	56	57	58
59	60	61	62	63	64	65	66	67	68	69	70
71	72	73	74	75	76	77	78	79	80	81	82
83	84	85	86	87	88	89	90	91	92	93	94
95	96	97	98	99	100	101	102	103	104	105	106
107	108	109	110	111	112	113	114	115	116	117	118
119	120	121	122	123	124	125	126	127	128	129	130
	131	132	133	134	135	136	137	138	139	140	

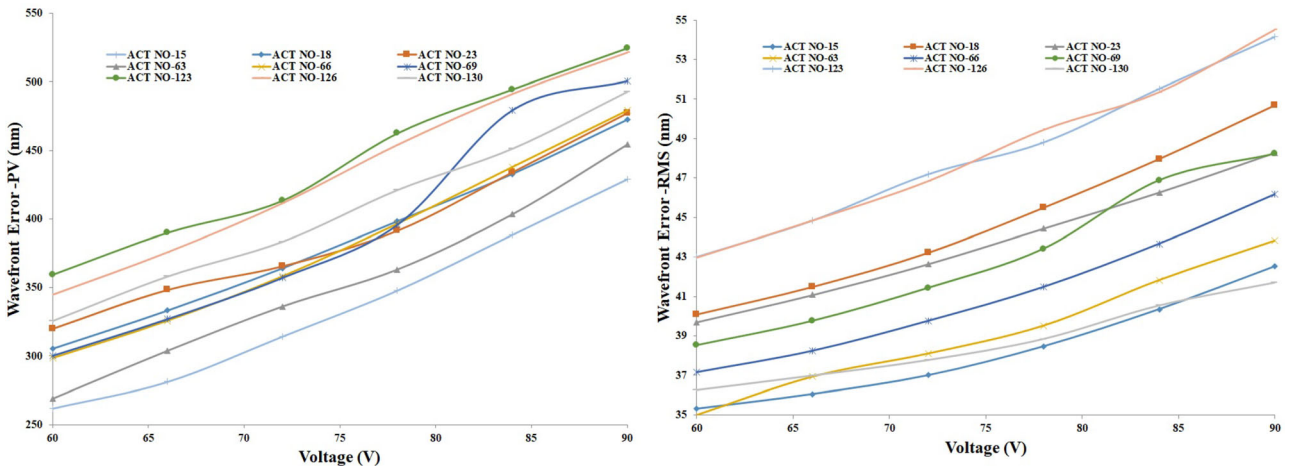

Fig. 9 Response of the DM actuators for input voltage. A set of actuators have been chosen from edges and central part for the analysis of their response to input voltage. Each data point is the mean value of 10 samples. The number of the actuators is labeled in the plot. PV (left) and RMS (right) response of wavefront is plotted

Table 2 DM actuators response matrix for variable "A" in Eq.4

0.04	0.15	0.06	0.12	0.12	0.03	0.03	0.02	0.04
0.10	0.12	0.07	0.11	0.07	0.03	0.03	0.01	0.05
0.10	0.10	0.11	0.11	0.06	0.02	0.05	0.03	0.07
0.05	0.09	0.06	0.08	0.05	0.09	0.04	−0.01	0.07
0.01	0.13	0.08	0.05	0.11	0.07	0.01	0.08	0.01
0.03	0.02	0.06	0.04	0.06	0.06	0.05	0.02	0.06
0.08	0.06	0.08	0.09	0.04	0.07	0.05	0.04	0.07
0.04	0.10	0.05	0.04	0.03	0.06	0.05	0.09	0.08
0.07	0.04	0.06	0.09	0.06	0.07	0.14	0.09	0.08

A second-order polynomial as shown in Eq. 6 is fitted to each of the actuator response (PV) for applied voltage over the range of 60-90 V. Coefficients of the polynomial are represented in a matrix form as shown in Tables 2, 3 and 4.

$$PV = Av^2 + Bv + C\,, \tag{6}$$

Equation 6 represents the response function of the DM. The coefficients A, B and C mentioned above are in matrix format. Here, v is the input voltage to the actuators and the PV is the peak-to-valley surface error of the DM. As mentioned earlier, the input voltage is in the range of 60-90 V and the PV is in nanometers.

From Fig. 9, it can be deduced that the individual actuator response is not similar for a given input voltage. This can be coupled with several factors. Those could be inter-actuator coupling effect, proximity of the actuators from the edge of DM, poor response of actuators.

Figure 10 shows the response of individual actuators at a given input voltage independently. The left column in this figure is the response in terms of PV, and the right column is RMS of the wavefront. The column number is labeled, and the actuator number is mentioned in the axis of the plot. For reference of the actuator position, Table 1 can be revisited.

Table 4 DM actuators response matrix for variable "C" in Eq.4

151.3	868.5	344.5	726.5	769.3	154.1	122.5	173.0	204.1
497.2	670.1	355.3	592.9	380.1	155.2	105.1	35.2	193.3
561.1	561.1	543.1	601.1	241.8	49.8	207.8	92.0	285.4
288.2	439.5	210.9	344.2	188.0	381.5	165.4	12.1	338.2
114.2	658.2	411.4	222.5	519.9	316.9	48.0	371.2	18.1
157.0	90.8	224.7	178.5	290.4	233.3	185.4	103.6	257.6
372.3	255.8	364.9	405.1	172.5	333.1	238.0	193.6	330.5
247.6	501.6	256.3	217.3	171.7	296.9	261.8	410.6	382.6
329.2	216.4	288.1	79.1	292.8	300.4	575.2	414.9	377.8

Table 5 Technical specifications of SHWS

Parameter	Value
Microlens diameter	150 μm
Microlens focal length	5.6 mm
Pixel size	6.5 μm
Number of microlenses	15x15 μm
Beam width	4 mm
Wavelength	633 nm
Tilt measurement	Image centroid shift
Wavefront reconstruction	Fried's reconstruction

Performance testing of DM using Zernike polynomials

The performance of DM is tested using standard Zernike polynomials [14, 15]. These aberrations are simulated and applied to deformable mirror as voltages. The response of the DM surface is measured by the interferometer. Standard Zernike polynomial is fitted to the measured DM surface map to estimate its response to the input. The Zernike polynomials are fit to a circular area of diameter $\sim$ 4 mm that covers 9x9 actuators on the DM surface. Here, it can be noted that system tilt, piston and power have been subtracted from all the results before fitting the polynomials. This is to minimize the static errors that can be due to instrument alignment and curvature effect of the lens. The test results are shown in Fig. 11. In this figure,

Table 3 DM actuators response matrix for variable "B" in Eq.4

−0.79	−19.02	−5.23	−15.25	−15.59	0.26	1.77	1.05	−0.68
−9.57	−13.91	−5.66	−11.85	−5.84	0.31	1.86	3.97	−1.07
−10.97	−11.13	−10.73	−12.16	−2.67	3.15	−1.20	1.79	−4.16
−2.81	−8.35	−2.14	−6.03	−1.14	−6.84	0.01	5.10	−5.03
1.92	−14.15	−7.29	−1.87	−10.49	−4.58	3.43	6.18	4.94
0.54	1.89	−2.19	−0.72	−3.49	−2.58	−0.89	2.40	−2.84
−6.10	−2.47	−5.53	−7.12	−0.25	−4.28	−1.70	0.86	−4.80
−0.62	−9.86	−1.75	−0.20	1.39	−2.90	−1.97	7.14	−6.16
−3.56	0.01	−2.87	−6.14	−2.58	−3.69	−13.49	7.00	−5.74

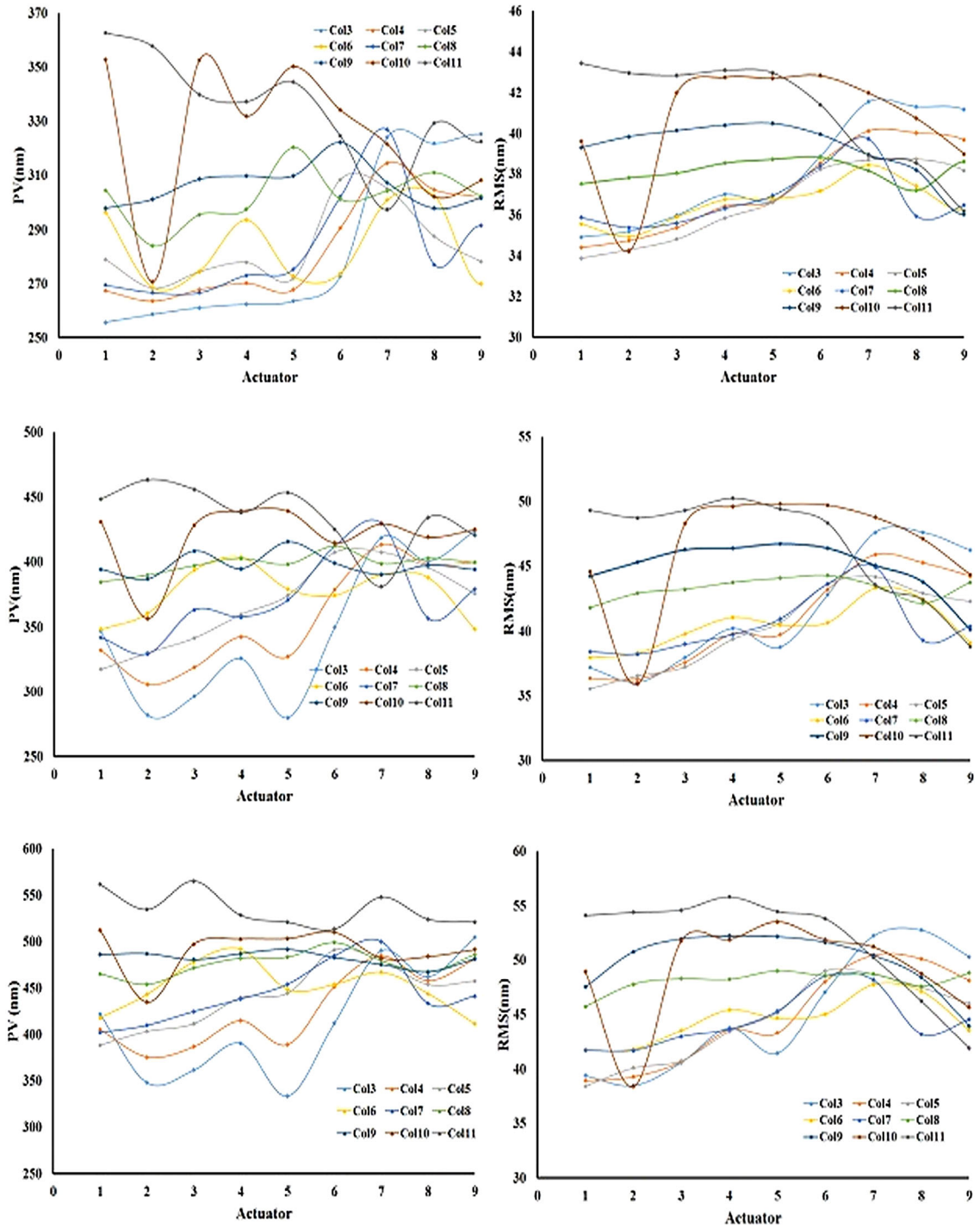

Fig. 10 Response of the individual actuators at different input voltages. The test voltages are 60V, 78 V and 90 V from top to bottom. The left column of the figure is peak to valley (PV) of the wavefront, and the right column is the root-mean-square (RMS) error of the wavefront

18x3 grid of images are shown. The left column is output wavefront of DM measured using interferometer, the middle column is the Zernike polynomial fit, and the last column is the residual after fitting.

In ideal scenario, for a given input Zernike, all the output Zernike terms should be zero except the input term. But in reality, all terms can never be zero. But, the dominant output term should be same as input. All the output Zernike is tabulated for a given input. This can be seen in Fig. 12. Along with the dominant terms, several other significant terms are present. The dominant Zernike coefficients are highlighted in red color. Figure 12 clearly

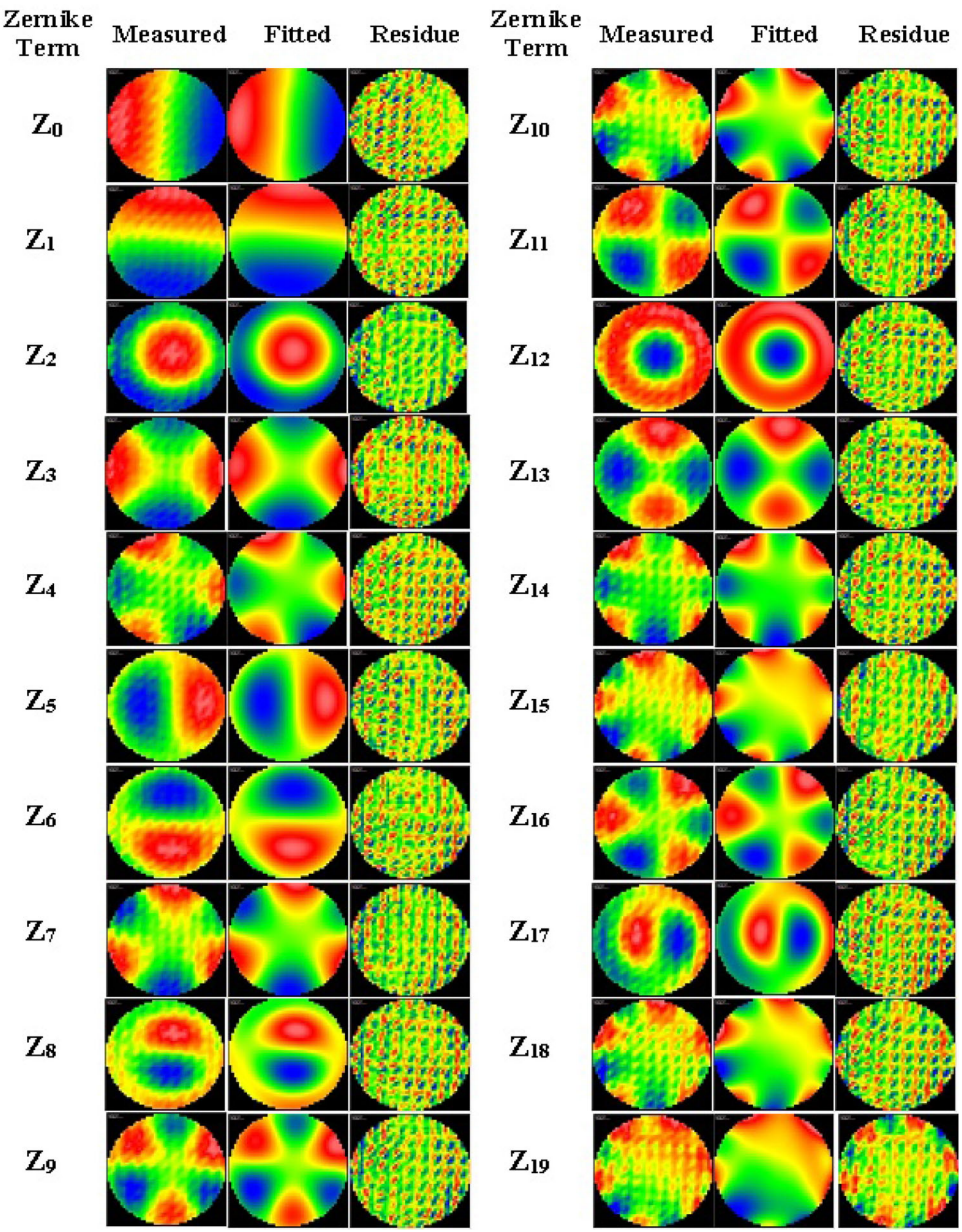

Fig. 11 The performance of deformable mirror is tested by using standard Zernike inputs. The response is tested over 10 Zernike orders. The left most column is resultant wavefront after Zernike input for the deformable mirror, center column is the Zernike fit, and the right column is the residual of the wavefront

shows that for a given input Zernike coefficient, same coefficient is dominated in the output. Along with expected output, some other terms are also dominant. These are highlighted in light blue color. There are several reasons for the presence of other terms. One among those are coupled Zernike terms. For example, coma (Z8, Z9) and tilt (Z1, Z2) are coupled and high-order astigmatism (Z13) is coupled with low-order astigmatism (Z5). This can be seen in Figs. 11 and 12 .

Calibration using Shack–Hartmann wavefront sensor (SHWS)

Shack–Hartmann wavefront sensor (SHWS) is an array of microlenses. This is an indisputable component to sense the distortions in a light wavefront because of its simplicity of installation and operation. It samples the wavefront at spatial scales equal to the diameter of the microlens. When a collimated wavefront is incident on the SHWS, each of the microlens forms an image. In ideal case, the images

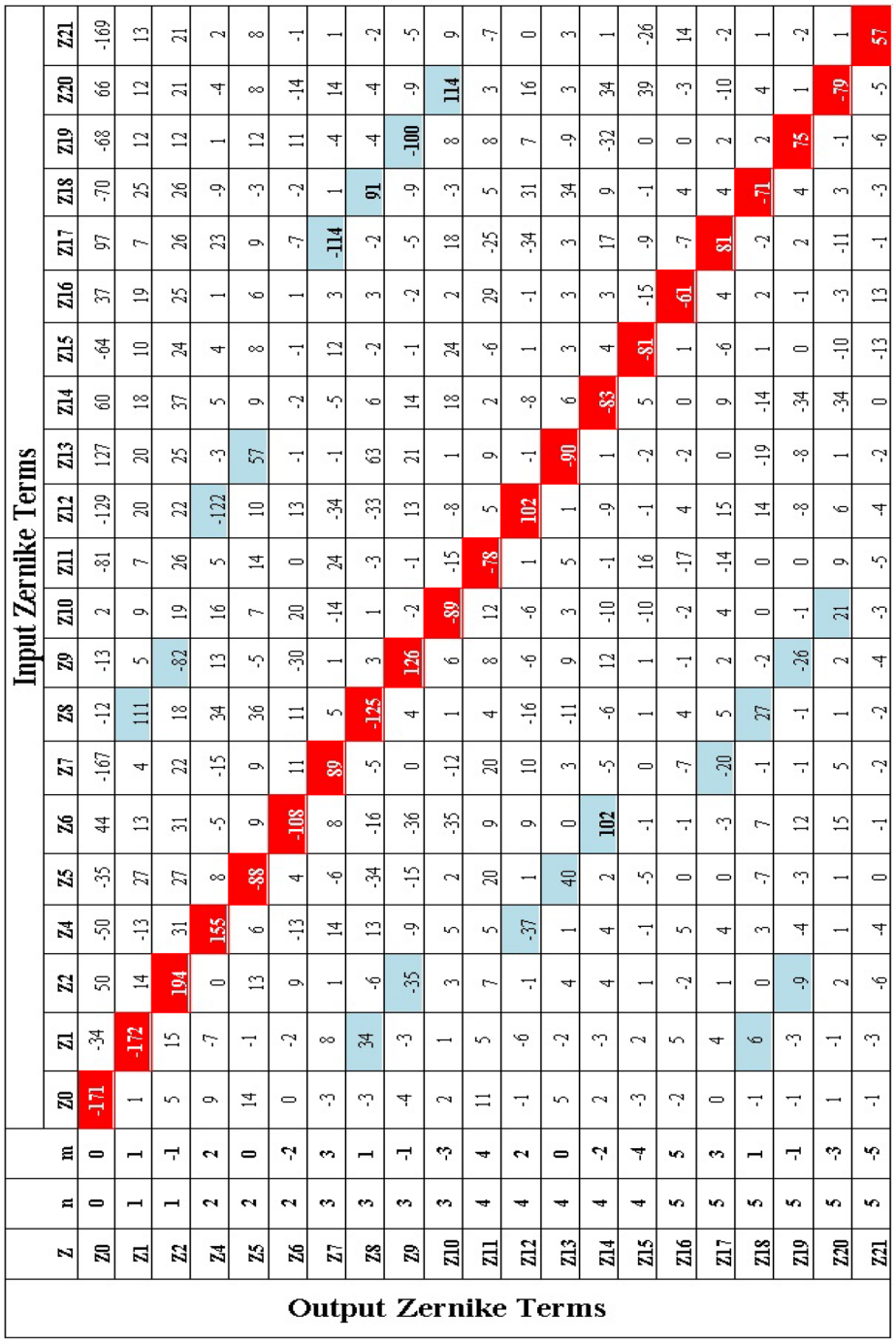

Fig. 12 The dominant Zernike output terms after fitting. Dominant terms are highlighted in red color. In all the cases, for the given input Zernike, the same are dominant in output. Some other dominant terms highlighted in light blue color. But these are either high-order or low-order terms of the same aberration

formed by each microlens of SHWS are uniformly distributed. The separation (in both X and Y directions) between the images will vary when a distorted wavefront is imaged. By measuring the drift in the image positions, distortions in the wavefront can be estimated. The sensitivity of the SHWS is dependent on the focal length and diameter of the microlens. An illustration of SHWS and its working principle for distorted and undistorted wavefronts is shown in Fig. 13.

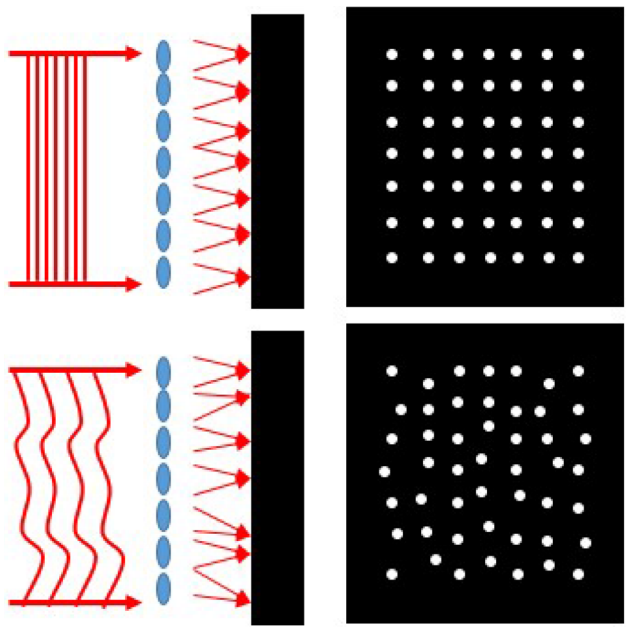

Fig. 13 Image formed by SHWS for an undistorted (top) and distorted (bottom) wavefront

SHWS is widely used in astronomical adaptive optics for sensing the wavefront distortions. The same is used to evaluate the performance of the AO subcomponents, namely phase plate and DM. A brief discussion about these components is made in the earlier sections of this paper. The following sections explain about calibration tests carried out on phase plate and DM using SHWS.

Calibration of phase plate using SHWS

Experimental setup for performance evaluation of phase plate using SHWS is shown in Fig. 14. A collimated beam of $\sim$ 4 mm diameter is transmitted through phase plate, and it is imaged using SHWS. The wavefront is reconstructed using drift in image positions at the focal plane of SHWS. The reconstructed wavefront and its one-dimensional plot can be seen in Fig. 15.

The same experiment is repeated for different regions on phase plate by rotating it. The RMS wavefront error obtained from these iterations is plotted in Fig. 16. The

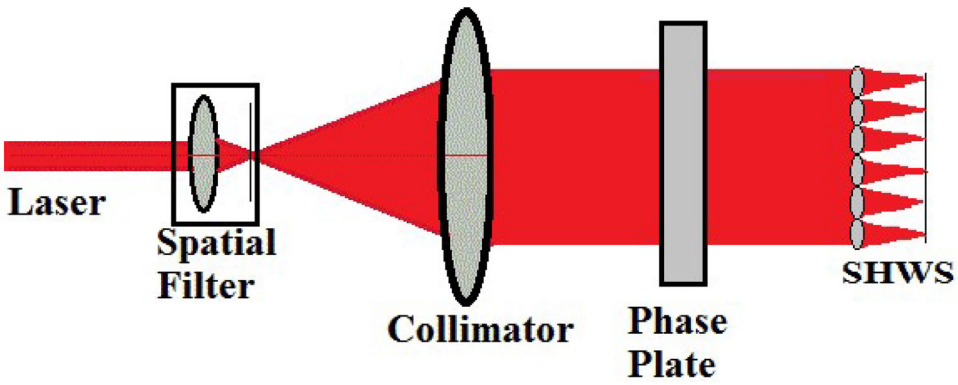

Fig. 14 Experimental setup for phase plate performance evaluation

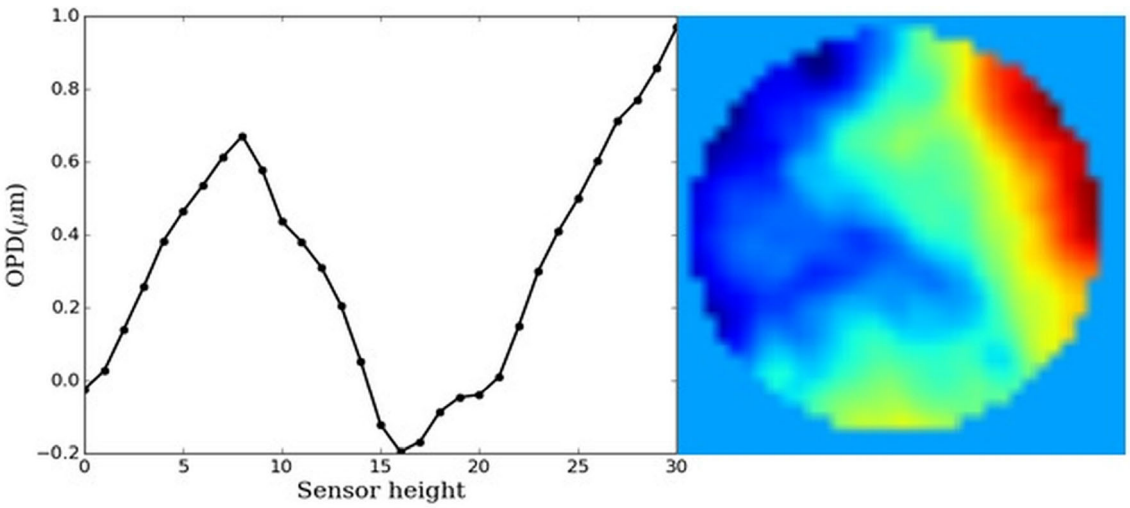

Fig. 15 Line plot of phase plate. It is tested over 5 mm diameter with 150 μm of sampling size. The horizontal axis shows the length in mm, and the vertical axis is optical path difference measured in μm

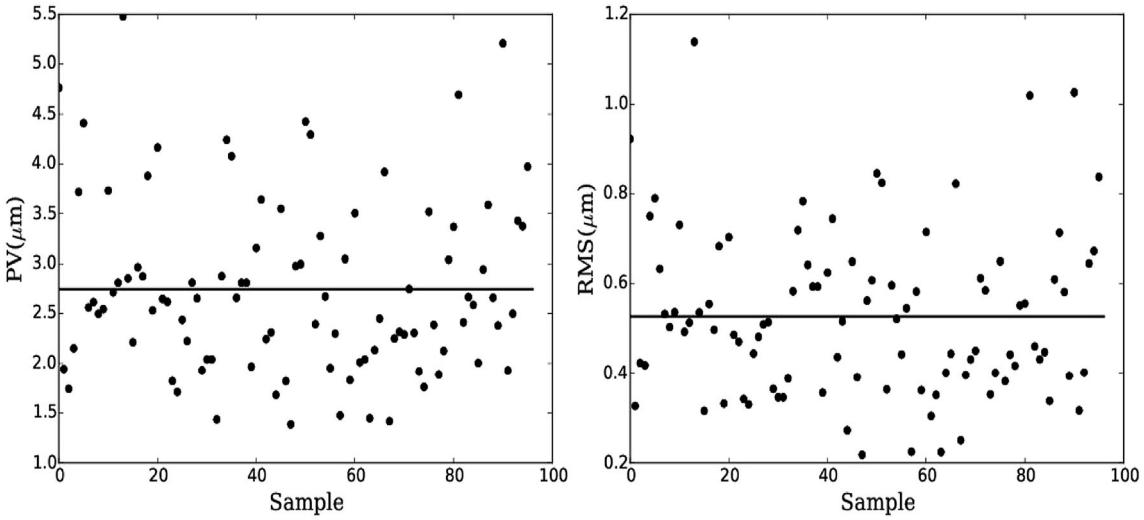

Fig. 16 PV and RMS optical path difference of phase plate. The data are collected randomly by rotating the phase plate. The data points are shown in dot marks, and the mean value of OPD is shown in solid line

Fig. 17 Experimental setup for deformable mirror performance evaluation

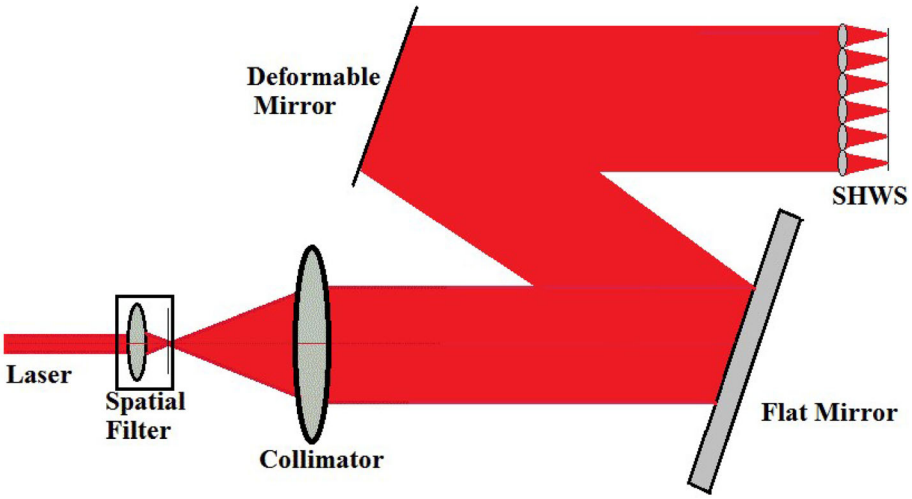

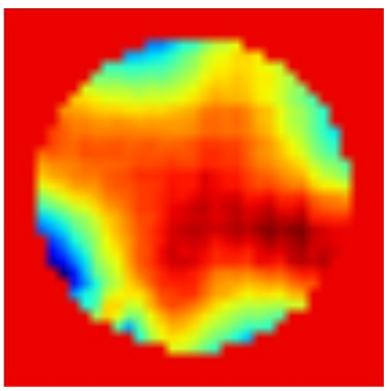

Fig. 18 Relaxed surface profile of DM

mean value of the RMS error is the resultant of ensemble average of the instantaneous RMS wavefront error.

The mean of RMS wavefront error induced by the phase plate is 0.263 μm. This value corresponds to Fried's parameter (r_o) of 12.19 cm on telescope of diameter of 1.3 m. The relation between Fried's parameter and wavefront distortions can be explained with the help of Eqs. 3, 4 and 5 .

Calibration of deformable mirror (DM) using SHWS

A brief introduction about DM, its specifications, operation and use is discussed in earlier sections. Current section mainly focuses on the tests carried out on DM to evaluate its performance by using SHWS.

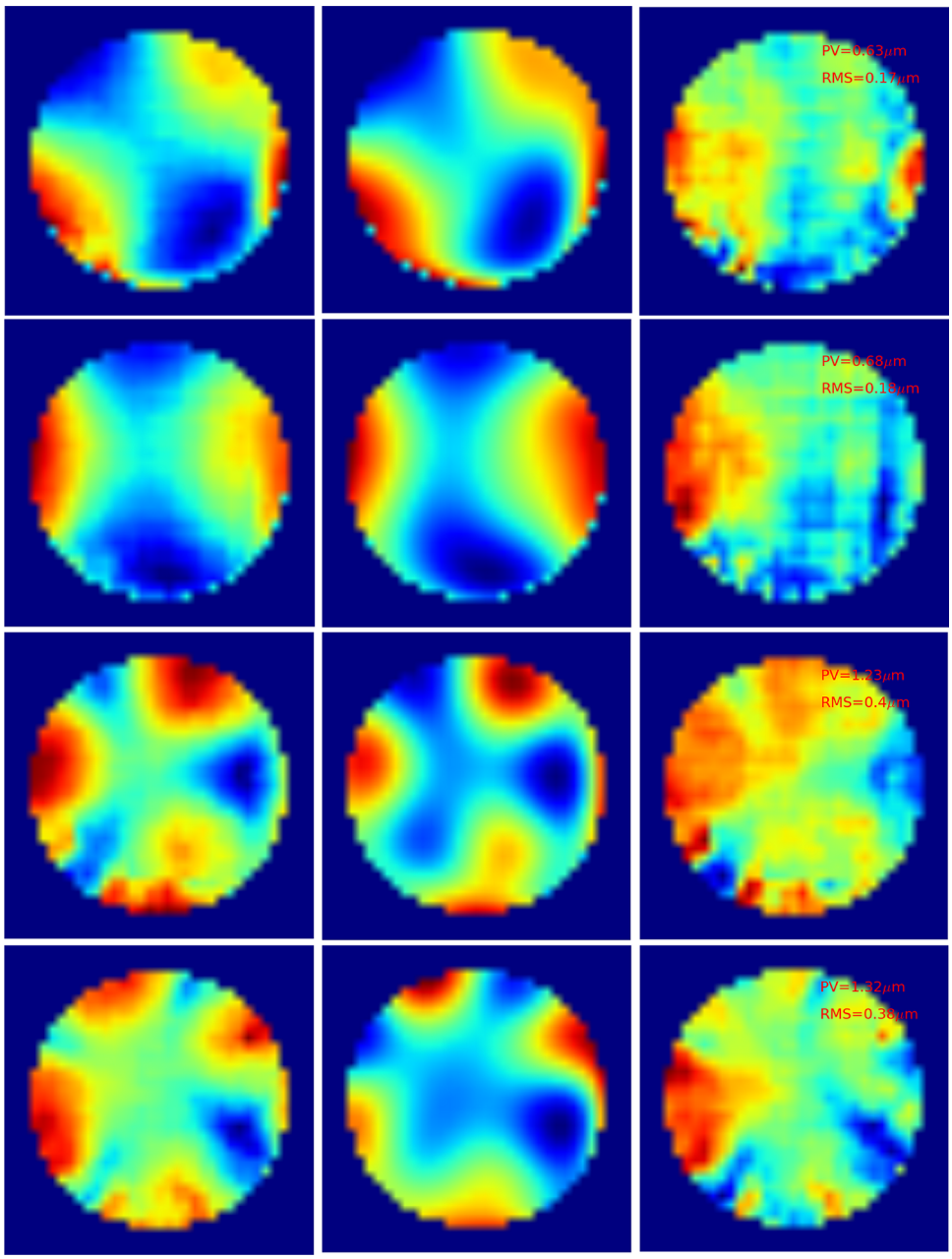

Fig. 19 Surface profile of DM for different Zernike coefficients. In this figure, the input Zernike (left), Zernike fit (center) and the residual (right) are shown. The row 1 to row 4 are for the input Zernike coefficients Z3, Z5, Z16, Z22, respectively

Experimental setup for calibrating the DM is shown in Fig. 17. Laser beam was spatial filtered and collimated by using a microscope objective, pinhole and a collimating lens. DM is placed in the path of the collimated beam. Reflected beam from the DM surface is imaged using SHWS. The drift in the image positions of the SHWS is used to reconstruct the wavefront of reflected beam from DM. The relaxed surface profile of DM is shown in Fig. 18.

SHWS measured response of DM for input Zernike polynomials

The input to DM and test conditions are same as described in Section 2.2.1. Here, the response of DM for given input Zernike is measured by using the SHWS. DM surface profile for few of input Zernike polynomials is shown in Fig. 19. From the reconstructed wavefront map of the DM surface, it is clear that the wavefront sampling is relatively

poor compared to the wavefront measurements carried out using Fizeau interferometer.

Discussion

Characterization of phase plate and deformable mirror (DM) is very crucial prior to the development of a prototype AO system. A highly sophisticated and reliable instrument is needed for such a characterization. Zygo Dynafiz is one of such systems that suits for this purpose. Calibration tests have been conducted on DM and phase plate using Zygo Dynafiz and SHWS.

In this characterization, it is estimated that the phase plate can induce wavefront distortions in the order of D/r_o in the range of 1 to 20 which can mimic seeing as minimum as 3 cm. The DM flatness is in the order of 20 nm as RMS error corresponds to a $\sim \lambda/30$ surface. It is good enough surface for atmospheric seeing corrections. The response of the actuators is fairly reliable. For a 30 V input voltage, PV is $\sim$ 250 nm and RMS with an accuracy of is $\sim$ 30 nm. So, this response is appreciably good for this purpose.

The DM performance is also tested over Zernike polynomials. The results show that the input Zernike is clearly dominated in the output. But for a given input Zernike coefficient, along with the dominant term some other coefficients are also having considerable values. The main reason for this could be the coupled coefficient effect of high-order Zernike with low-order Zernike.

Characterization of DM and phase plate is also carried out by using SHWS. The test results obtained for phase plate are similar in both cases, i.e., Fizeau interferometer and SHWS. In case of DM surface wavefront measurements for input Zernike, the difference between Fizeau interferometer and SHWS is more evident. The DM surface profile measured using SHWS for higher-order Zernike is mostly effected due to the limited spatial sampling of SHWS which is 150 μm, whereas the DM surface profile measured using Fizeau interferometer is more accurate as compared. This is mainly due to the better spatial sampling of the interferometer which is 5.5 μm.

From this characterization, it can be concluded that phase plate Lexitek LS100 and Boston Multi-5.5 DM are suitable for developing the working laboratory model of higher-order AO system.

References

1. J.W. Hardy, *Adaptive optics for astronomical telescopes* (Oxford University Press, Oxford, 1998)
2. T. Robert, *Principles of adaptive optics* (CRC Press, Florida, 2010)
3. D.L. Fried, Limiting resolution looking down through the atmosphere. J. Opt. Soc. Am. **56**, 1380–1384 (1996)
4. V. I. Tatarskii, The effects of the turbulent atmosphere on wave propagation. Israel Program for Scientific Translations. Jerusalem (1971)
5. J.M. Beckers, Adaptive optics for astronomy - Principles, performance, and applications. Ann. Rev. Astron. Astrophys. **31**, 13–62 (1993)
6. M. A. Van Dam, B. A. Macintosh, Characterization of adaptive optics at Keck Observatory. Proc. SPIE. Astronomical Adaptive Optics Systems and Applications. 5169, 1-10 (2003)
7. D. M. Sykora, M. L. Holmes, Dynamic measurements using a Fizeau interferometer. Proc. SPIE. Optical Measurement Systems for Industrial Inspection VII. 8072, 537-546 (2011)
8. M. Girija, S. Rina, K. Usha, K.P. Chaudhary, Evaluation of measurement uncertainty for absolute flatness measurement by using Fizeau interferometer with phase-shifting capability. Mapan **29**, 261–267 (2014)
9. P.F. Forman, The Zygo interferometer system. Proc. SPIE. Interferometry. **192**, 41–49 (1979)
10. S. M. Ebstein, Pseudo-random phase plates. Proc. SPIE. High-Resolution Wavefront Control: Methods, Devices, and Applications III. 4493, 150-155 (2002)
11. D.L. Fried, Optical resolution through a randomly inhomogeneous medium for very long and very short xposures. J. Opt. Soc. Am. **56**, 1372–1379 (1996)
12. A. Raja Bayanna, R.E. Louis, S. Chatterjee, S.K. Mathew, P. Venkatakrishnan, Membrane-based deformable mirror: intrinsic aberrations and alignment issues. Appl. Opt. **54**, 1727–1736 (2015)
13. S. Cornelissen, P. A. Bierden, T. Bifano, MEMS deformable mirrors for adaptive optics in astronomical imaging. The Advanced Maui Optical and Space Surveillance Technologies Conference (2006)
14. R.J. Noll, Zernike polynomials and atmospheric turbulance. J. Opt. Soc. Am. **66**, 207–211 (1976)
15. J.Y. Wang, D.E. Silva, Wavefront interpretations with Zernike polynomials. Appl. Opt. **19**, 1510–1518 (1980)